HHS Public Access

Author manuscript

Neuroimage. Author manuscript; available in PMC 2022 October 19.

Published in final edited form as:

Neuroimage. 2022 July 15; 255: 119180. doi:10.1016/j.neuroimage.2022.119180.

Longitudinal surface-based spatial Bayesian GLM reveals complex trajectories of motor neurodegeneration in ALS

Amanda F. Mejia[a,*], **Vincent Koppelmans**[b], **Laura Jelsone-Swain**[c], **Sanjay Kalra**[d], **Robert C. Welsh**[b,e]

[a]Department of Statistics, Indiana University, Bloomington, IN, USA

[b]Department of Psychiatry, University of Utah, Salt Lake City, UT, USA

[c]Department of Psychology, University of South Carolina Aiken, Aiken, SC, USA

[d]Division of Neurology, Department of Medicine, University of Alberta, Edmonton, AB, Canada

[e]Department of Psychiatry and Biobehavioral Sciences, University of California Los Angeles, Los Angeles, CA, USA

Abstract

Longitudinal fMRI studies hold great promise for the study of neurodegenerative diseases, development and aging, but realizing their full potential depends on extracting accurate fMRI-based measures of brain function and organization in individual subjects over time. This is

*Corresponding author. afmejia@iu.edu (A.F. Mejia).

Credit authorship contribution statement

Amanda F. Mejia: Conceptualization, Methodology, Software, Validation, Formal analysis, Resources, Writing – original draft, Visualization, Funding acquisition. **Vincent Koppelmans:** Data curation, Writing – review & editing, Visualization. **Laura Jelsone-Swain:** Investigation, Writing – review & editing. **Sanjay Kalra:** Writing – review & editing. **Robert C. Welsh:** Conceptualization, Investigation, Validation, Formal analysis, Resources, Data curation, Writing – original draft, Visualization, Supervision, Funding acquisition.

Data and Code Availability Statement

"Longitudinal surface-based spatial Bayesian GLM reveals complex trajectories of motor neurodegeneration in ALS " by Amanda F. Mejia, Vincent Koppelmans, Laura Jelsone-Swain, Sanjay Kalra, and Robert C. Welsh.

Code:

All data analysis was performed using version 4.0.3 of the R open-source software.1 All packages listed below are available via CRAN or Github. In the latter case, links are provided below. All packages can be directly installed from within R using the code provided. The BayesfMRI package (version 0.1.8)2 was used to implement the longitudinal surface-based spatial Bayesian GLM to identify areas of activation during task. The gifti package (version 0.8.0) was used to read in GIFTI-format cortical surface geometry files. The fMRIscrub package (version 0.3.0)3 was used for data-driven scrubbing and quality control. The cifti-Tools package (version 0.3.1)4 was used for visualization of results on the cortical surface. ciftiTools requires installation of the Connectome Workbench.5 Longitudinal mixed-effects modeling was performed using the lme4 package (version 1.1–25), and splines were fit using the splines package (version 4.0.3). All code used to perform the data analyses presented in this paper is available at the following Github repository: https://github.com/mandymejia/ALS-BayesianGLM-paper/.

Data:

We have included 1 participant's dataset in the Github repository listed above (120 megabytes). This allows interested individuals to download and test the Bayesian GLM code. Summary measures from the GLM for all subjects are also available through the Github repository, allowing interested parties to reproduce the figures from the paper. Upon request we can then make the remaining data available for interested parties directly. The full dataset is approximately 4 gigabytes. Due to our Institutional Review Board-approved protocol we are limited to only making data available that is stripped of all identifiers as well as any biometrics (such as the participant's face that could be reconstructed from a high-resolution 3D T1-weighted image). We are therefore able to share surface-projected fMRI data, along with the surface models derived from our custom pre-processing pipeline.

Supplementary material

Supplementary material associated with this article can be found, in the online version, at doi: 10.1016/j.neuroimage.2022.119180.

especially true for studies of rare, heterogeneous and/or rapidly progressing neurodegenerative diseases. These often involve small samples with heterogeneous functional features, making traditional group-difference analyses of limited utility. One such disease is amyotrophic lateral sclerosis (ALS), a severe disease resulting in extreme loss of motor function and eventual death. Here, we use an advanced individualized task fMRI analysis approach to analyze a rich longitudinal dataset containing 190 hand clench fMRI scans from 16 ALS patients (78 scans) and 22 age-matched healthy controls (112 scans) Specifically, we adopt our cortical surface-based spatial Bayesian general linear model (GLM), which has high power and precision to detect activations in individual subjects, and propose a novel longitudinal extension to leverage information shared across visits. We perform all analyses in native surface space to preserve individua anatomical and functional features. Using mixed-effects models to subsequently study the relationship between size of activation and ALS disease progression, we observe for the first time an inverted U-shaped trajectory o motor activations: at relatively mild motor disability we observe enlarging activations, while at higher levels of motor disability we observe severely diminished activation, reflecting progression toward complete loss of motor function. We further observe distinct trajectories depending on clinical progression rate, with faster progressors exhibiting more extreme changes at an earlier stage of disability. These differential trajectories suggest that initial hyper-activation is likely attributable to loss of inhibitory neurons, rather than functional compensation as earlier assumed. These findings substantially advance scientific understanding of the ALS disease process. This study also provides the first real-world example of how surface-based spatial Bayesian analysis of task fMRI can further scientific understanding of neurodegenerative disease and other phenomena. The surface-based spatial Bayesian GLM is implemented in the BayesfMRI R package

Keywords

Bayesian; Statistics; Longitudinal; General linear model; Neurodegeneration

1. Introduction

Longitudinal fMRI studies are a powerful tool for examining functional brain changes occurring within individuals in the context of neurodegenerative diseases, development and normal aging (Telzer et al., 2018). Longitudinal studies can account for measures reflective of heterogeneity between and across participants over time (e.g., disease burden) (Kassubek et al., 2014; Lawrence et al., 2017) and are key for the development of biomarkers (Turner and Modo, 2010), an area of ongoing interest and development in neuroimaging research (Woo et al., 2017).

To utilize longitudinal fMRI datasets to their full potential, it is critical to develop and employ statistical methods for accurate individual-level analysis, rather than traditional group-average and group-difference analysis. This is particularly true for longitudinal studies of rare, heterogeneous and/or rapidly progressing neurodegenerative diseases — which are often difficult and expensive to acquire —as they typically involve small numbers of participants whose functional brain features may vary markedly across subjects and over time. Individualized analytical methods would facilitate the use of such studies to understand

the dynamics of neurodegeneration, to develop neuroimaging biomarkers, and to ultimately translate research findings to monitor disease progression and evaluate treatment efficacy clinically. Individualized analyses are also less likely than group-average analyses to require spatially warping participants' brains to a standard template. Such warping or normalization can induce errors and inaccuracies, particularly in individuals with neurodegenerative disease and even in normal aging (Eloyan et al., 2014; Kolinger et al., 2021).

Individual-level estimates of activation based on conventional task fMRI analysis methods have unfortunately been found to exhibit poor reliability (Elliott et al., 2020), in part due to sub-optimal statistical approaches (Monti, 2011). By far the most popular method for task fMRI analysis is the classical general linear model (GLM) (Worsley and Friston, 1995). In this massive univariate approach, at the first level a separate linear model is fit at every voxel relating the observed BOLD activity to the expected response to each task or stimulus. At the second level, participant-level estimates are pooled to produce group average estimates of activation or differences between groups or conditions. Historically, the classical GLM has been considered sufficient in group-average fMRI studies, where the focus is on estimation of robust effects that are common across most participants (Mumford and Nichols, 2009). However, effects that are unique to individuals or states are likely to be washed out in a group analysis (Gupta et al., 2010; Stern et al., 2009), and the classical GLM has been shown to have low estimation efficiency and power for subject-level analysis (Mejia et al., 2020). Additionally, many task fMRI analyses are performed in volumetric space, which has a number of drawbacks, including smoothing across tissue classes and distal cortical areas representing distinct functional regions (Brodoehl et al., 2020).

Here, we adopt and extend our advanced individualized fMRI analysis approach, the cortical surface-based spatial Bayesian GLM (Mejia et al., 2020), to better understand the longitudinal disease process in amyotrophic lateral sclerosis (ALS), a rare, rapidly progressing and heteroegenous neurodegenerative disease. This approach avoids data smoothing, leverages spatial dependencies along the cortical surface, and avoids the need for multiplicity correction —and the resulting loss of power —in identifying areas of activation. It yields substantially more accurate and powerful activations in individual subjects (Mejia et al., 2020). We propose a novel longitudinal model extension, which leverages information shared across multiple visits. Our analyses are performed entirely in native space to preserve the unique anatomical and functional features of each participant (Gray et al., 2012; Kolinger et al., 2021), using the size of activations above a certain effect size as a summary measure that can be used in subsequent longitudinal analysis.

Specifically, we analyze a rich longitudinal study including 78 motor task fMRI scans from 16 ALS participants and 112 scans from 22 age-matched healthy control (HC) participants. Most ALS participants were enrolled soon following clinical diagnosis, and follow-up scans occurred roughly every 3 months for as long as participants were willing and able to participate in the study. This study is unique in terms of the high frequency and long duration of sampling, providing an opportunity to understand how disease progression evolves dynamically in different individuals. We apply our longitudinal surface-based spatial Bayesian GLM to each participant's data and extract summary measures of activation at each visit. We then analyze these summary measures using a series of longitudinal mixed

effects models to study the relationship between brain activation and functional disability in ALS over time.

Previous studies have documented ALS-related motor disruptions using a variety of measures, including task activation (Konrad et al., 2002; 2006; Poujois et al., 2013; Schoenfeld et al., 2005; Stoppel et al., 2014), functional connectivity (Jelsone-Swain et al., 2010; Menke et al., 2018), cortical thickness (Agosta et al., 2012; Verstraete et al., 2010), and structural connectivity (Chapman et al., 2014; Douaud et al., 2011; Menke et al., 2012; Müller et al., 2016). Task activation studies specifically have observed hyper-activation in patients with ALS during motor tasks (Konrad et al., 2002; Poujois et al., 2013; Schoenfeld et al., 2005). However, since these studies have been based on more limited sampling designs (Menke et al., 2018) and employed group-average analysis approaches, they provide limited insight into the heterogeneous and typically rapid disease process characterizing ALS.

Our longitudinal analyses reveal an inverted U-shaped trajectory of motor activation associated with disease progression in ALS, with hyper-activation initially occurring at relatively low levels of motor disability, followed by dramatic loss of activation occurring at with more severe motor disability. To our knowledge, this is the first time this inverted U-shaped trajectory has been observed in ALS. Further, we observe systematic differences by clinical progression rate, with fast progressors exhibiting more extreme hyper-activation and more severe loss of activation earlier in the disease process. Despite the long-standing interest in spatial Bayesian techniques for task fMRI analysis (Friston and Penny, 2003, 2007; Woolrich et al., 2009), to our knowledge this is the first study of neurodegenerative disease that has employed a surface-based spatial Bayesian GLM, and illustrates the power of this approach to extract new scientific insights, especially when applied to rich longitudinal fMRI studies.

2. Materials and methods

2.1. Participants

ALS participants were recruited through the University of Michigan ALS clinic and had been diagnosed as having probable or definite ALS per the El Escorial Criteria (Brooks, 1994). The project was approved by the University of Michigan Institutional Review Board (HUM00000219). All participants gave written informed consent before participation. Healthy controls were recruited from the local community through community advertising and were balanced on age. Participants underwent magnetic resonance imaging (MRI) at multiple research visits. For convenience for the ALS participants, research visits were scheduled to coincide with clinical visits. Visits were scheduled at roughly 3-month intervals while minimizing travel burden to participants with ALS. Participants with ALS continued into the study until they could no longer tolerate the MRI session, decided on their own accord to no longer participate, or passed away. The sample used for analysis included 190 scanning visits from 16 ALS participants (78 visits) and 22 HC participants (112 visits). ALS patient demographics are given in Table 1. The number of visits per participant ranged from 3 to 10 (median = 4.5, mean = 5). Participants' visit timing is shown in Supplementary Fig. A1. Healthy control participant demographics are given in Supplementary Table A1.

At the time of each scanning visit, ALS participants had function assessed with the ALS Functional Rating Scale (revised) (ALSFRS-R), a standard instrument that is widely used in clinical care and clinical research (Rooney et al., 2017). ALSFRS-R scores range from 48 (no impairment) to 0 (total impairment). Fig. 1 displays ALSFRS-R trajectories for each ALS participant in the study, and Supplementary Table A2 shows ALSFRS-R scores at the first and last visit for each participant. All but two participants had ALSFRS-R scores over 35 at the first visit, indicating a relatively mild disease state. Fig. 1 shows that many ALS participants experienced wide range of disability levels through the course of the study.

2.2. MRI data collection

MRI data were collected on a GE 3T Excite 2 scanner (General Electric, Milwaukee, Wisconsin). A high-resolution T_1-weighted image was acquired (3D SPGR, IR 500ms, 15° flip angle, TR = 9.036ms, TE = 1.84ms, 256×256 ×160 matrix, 1.102×1.102 ×1.2 mm resolution). For image coregistration, we also collected a lower resolution T_1-weighted image (85° flip angle, TR = 250ms, TE = 5.70ms, 256 ×160 matrix, 3mm slice thickness and no skip) at the same spatial locations as the functional time-series data. Blood oxygenation level dependent (BOLD) data were collected using a reverse-spiral k-space trajectory sequence (Noll, 2002), and reconstructed off-line using a gradient descent algorithm (Noll et al., 2004).

BOLD fMRI data were collected for 4 tasks: right hand finger tapping, right first clenching, left hand finger tapping, and left fist clenching. All tasks used a paced-block design, in which a visual target appeared every 1.5 seconds for the participant to execute the given task. This visual cue appeared 20 times in each block, followed by 15 seconds of a fixation cross-hair. A block design was used for robustness and less sensitivity to variation in the hemodynamic response across individuals (Liu et al., 2001; Shan et al., 2013). Task difficulty was matched on hand-strength. Just prior to the scan, participants had their hand strength measured 3 times with a dynanometer (Jamar Hydraulic Hand Dynanometer, Model SD081028935). In the scanner, participants squeezed a resistive hand exerciser (Sammons-Preston Model 56573) set to approximately 10% of their mean measured hand strength. The task was practiced outside the scanner to ensure participant compliance. The block-rest cycle was repeated for a total of 6 times. Each BOLD time-series run was limited to a single task, resulting in 4 separate runs. BOLD data were collected with a T_2^* -weighted gradient-echo, spiral-readout sequence (90° flip angle, TR = 2s, TE = 30ms, 64×64 matrix, 3 mm slice thickness and no skip, 220mm field-of-view, sequential and ascending acquisition, 40 slices). The first four T_2^* volumes at the beginning of the time-series sequence were excited but not recorded to allow for magnetization equilibrium. We limit analyses to the right hand first clenching task, since clenching is simpler to execute than the more complex finger tapping sequence (index-to-thumb followed by middle-to-thumb) and more participants were able to complete the right hand tasks.

2.3. Image processing

We constructed a custom pipeline to process the BOLD time series to the cortical surface for statistical analysis. The goal of this pipeline was to produce surface BOLD time-series

data registered to a participant-specific template to allow for longitudinal modeling of co-registered visits for a given participant, while respecting participant-specific cortical anatomy for more accurate spatial dependence modeling in the Bayesian analysis described in Section 2.4 below.

First, the BOLD data were slice-time corrected, realigned, and registered to the N4 non-uniformity corrected T_1-weighted structural scan. A participant template was created based on the bias field corrected T_1-weighted images of all sessions using iterative rigid body registration through Advanced Normalization Tools (ANTs)(Avants et al., 2011). For each participant, this template was processed through FreeSurfer (Fischl, 2012) to result in a model of the pial surface and a corresponding spherical surface. No data smoothing was performed, since the spatial Bayesian model implicitly smooths task activation maps at an optimal level (see Section 2.4.1 and Supplementary Section C for more information). For additional details on BOLD and surface processing, including registration, bias field correction, and surface projection, see Supplementary Section B.

A participant-specific sensorimotor mask consisting of four FreeSurfer sensorimotor areas was constructed to limit the location of statistical estimation. To reduce computational load of Bayesian model estimation without significant loss of spatial resolution, we resampled the pial surfaces, BOLD data, and masks to 10,000 vertices per hemisphere. After applying the sensorimotor masks, we are left with approximately 1500 vertices per hemisphere. Supplementary Fig. C4 displays the resampled pial surfaces and mask for each hemisphere for one individual with ALS.

We identified and removed highly noisy volumes and sessions based on a data-driven scrubbing technique (Mejia et al., 2017), resulting in exclusion of six sessions in total (see Supplementary Section B for details). Prior to model fitting, we centered and scaled the BOLD data to units of local percent signal change. We also regressed nuisance signals from the fMRI data and design matrix, including the six rigid body realignment parameters, their first derivatives, and linear and quadratic trends. This was done prior to model fitting, since the computational complexity of model fitting in our spatial Bayesian model increases with each additional design matrix column.

2.4. Statistical analysis

The block design for right hand clenching was convolved with a canonical hemodynamic response function (HRF), a double gamma-variant function (Shan et al., 2013). We also included the temporal derivative of the task stimulus function to allow for differences in HRF onset timing across the brain, participants and visits (Supplementary Fig. B3). No prewhitening was performed, since inspection of the residuals revealed little to no temporal dependence, likely due to the relatively long TR and inclusion of the HRF derivative.

We fit a longitudinal spatial Bayesian GLM, described next, to produce estimates of activation amplitude and areas of activation for each participant and each visit. The model was fit within each hemisphere's cortical surface separately. Areas of activation were based on the joint posterior distribution of activation amplitude, while controlling the family-wise

error rate (FWER) at a significance level of $\alpha = 0.05$. We computed the total size of activation by summing the surface area associated with each vertex identified as activated.

For comparison, we also fit a classical "massive univariate " GLM, including identifying areas of activation by performing a t-test at every location. We corrected for multiplicity within each hemisphere using Bonferroni correction to control the FWER and the Benjamini-Hochberg procedure (Benjamini and Hochberg, 1995) to control the false discovery rate (FDR). Note that while Bonferroni correction is often considered overconservative in traditional whole brain analysis, here we are performing a much smaller number of tests (approximately 1500 per hemisphere). A significance level of $\alpha = 0.05$ was used, as in the spatial Bayesian GLM.

2.4.1. Longitudinal spatial Bayesian modeling—We adapted the spatial Bayesian GLM proposed by Mejia et al. (2020) for analysis of task fMRI on the cortical surface. The original model was designed for single-subject, single-session analysis. We proposed a novel longitudinal extension to allow for subject- and visit-specific estimation and areas of activation, while leveraging information shared across visits. The details of this model are described in Supplementary Section C. Briefly, the spatial Bayesian GLM leverages similarities in activation patterns across the cortex, resulting in smoother, more accurate estimates and areas of activation compared with a massive univariate approach (Mejia et al., 2020). The smoothness (spatial correlation range) of the spatial prior associated with the latent fields for each task is estimated through the model, so that the optimal degree of smoothing is applied to each field via the prior. In addition, the Bayesian model has high power to identify areas of activation. Instead of the traditional approach of hypothesis testing followed by multiple comparisons, this model utilizes the joint posterior distribution of activation to identify a single set of locations that have high probability of being activated, achieving FWER control.

The high statistical power of the spatial Bayesian GLM may result in a phenomenon where large areas of low effect size are deemed significantly activated (Cremers et al., 2017). Therefore, a scientifically relevant effect size, γ, is often specified to avoid detecting irrelevant activations. For example, an effect size of $\gamma = 1\%$ can be adopted to identify only locations that exhibit $> 1\%$ local signal change due to the task. An effect size of $\gamma = 0\%$ would correspond to the traditional hypothesis testing framework used in the classical GLM. Here, we consider three effect sizes: $\gamma = 0\%$, 1% and 2%.

Model fitting was performed in using the BayesfMRI R package (version 1.8) (https://github.com/mandymejia/BayesfMRI/).

2.4.2. Relating size of activation to disability—To examine the relationship between size of motor activation and ALS disability, we fit a series of random intercept models for each effect size γ and each hemisphere (left/right). To avoid the undue influence of temporal outliers on the regression fit, we limited ALS participant data to a 2-year window of maximal change in ALSFRS-R. This resulted in removal of the first visit for participant A14 (Fig. 1). Additionally, participant A04 had a very slow disease trajectory compared with the typical survival time in ALS (Fig. 1) and many visits spanning a long

duration (Fig. A1). Since this atypical ALS case is not representative of the population, this participant's data was excluded from model fitting. Robustness checks including subject A04 and including all visits from all subjects are given in Supplementary Section F. The results of those checks show that our findings are robust to these exclusions. We controlled for participant sex and age at first scan in each model described below, since these have been shown to be related to disease progression in ALS (Murdock et al., 2021).

In lieu of time since symptom onset, given the heterogeneity of the rate of disease progression, we constructed three predictors related to disability in ALS, adopting from Rooney et al. (2017) : *Total Disability* $\left(D_{ij}^{tot}\right)$, *Hand Motor Disability* $\left(D_{ij}^{hand}\right)$ and *Other Disability* $\left(D_{ij}^{oth}\right)$. For participant i at visit j,

$$D_{ij}^{tot} = 1 - \frac{ALSF\,RS_{ij}}{48}, \quad D_{ij}^{hand} = 1 - \frac{ALSF\,RS_{ij}^{hand}}{12}, \quad \text{and } D_{ij}^{oth} = 1 - \frac{ALSF\,RS_{ij}^{other}}{36}, \tag{1}$$

where $ALSFRS_{ij}$ is the total ALSFRS-R score; $ALSF\,RS_{ij}^{hand}$ is the sum of three ALSFRS-R item scores for tasks related primarily to hand function: handwriting, cutting (with or without gastronomy), and dressing/hygiene; $ALSF\,RS_{ij}^{other}$ is the sum of the nine remaining ALSFRS components (speech, salivation, swallowing, turning in bed and adjusting bed clothes, walking, climbing stairs, dyspnea, orthopniea, and respiratory insufficiency). The denominator of each term is the maximum possible score. Thus, D_{ij}^{tot}, D_{ij}^{hand} and D_{ij}^{oth} each range from 0 (no disability) to 1 (total disability).

Let A_{ij} be the size of the area of activation above a given effect size for participant i at visit j. The total disability random intercept model for the ALS group is

$$A_{ij} = \beta_0 + b_{0i} + \beta_1 age_i + \beta_2 sex_i + f\left(D_{ij}^{tot}\right) + \epsilon_{ij}, \quad \epsilon_{ij} \sim N\left(0, \sigma^2\right), \tag{2}$$

where β_0 represents the average size of activation when *Total Disability* is zero; b_{0i} represents the random deviation for subject i; and the spline function $f(\cdot)$ allows for a non-linear relationship between *Total Disability* and activation size (see Supplementary Section B for more information about the construction of the spline). The hand motor disability model for the ALS group is

$$A_{ij} = \beta_0 + b_{0i} + \beta_1 age_i + \beta_2 sex_i + f\left(D_{ij}^{hand}\right) + \beta_3 D_{ij}^{oth} + \epsilon_{ij}, \quad \epsilon_{ij} \sim N\left(0, \sigma^2\right), \tag{3}$$

where β_0 represents the average size of activation when *Hand Motor Disability* and *Other Disability* are both zero; b_{0i} represents the random deviation for subject i; β_3 represents the average change in size of activation associated with a 1-unit increase in *Other Disability*. The spline function $f(\cdot)$ allows for a non-linear relationship between *Hand Motor Disability* and activation size. This model form, including the choice of a non-linear spline for *Hand Motor Disability*, was determined by a series of likelihood ratio tests (LRTs) (Supplementary Section B). Alternative model formulations were substantially

worse in terms of predictive accuracy and Akaike information criterion (AIC) (Akaike, 1998). This suggests that the non-linear relationship between *Hand Motor Disability* and size of activation is not a spurious result of over-fitting, but rather is statistically significant based on the evidence in the data. Note that these models incorporate both longitudinal data sources on participants with ALS: brain activation (fMRI) and disability (ALSFRS-R).

To investigate the role of disease progression on the relationship between size of activation in disability in ALS, we divided subjects into three groups of progressors based on their progression rate (Ellis et al., 1999): fast, moderate and slow (see Table 2). Only one participant (A04) was classified as a slow progressor. We therefore limited this analysis to a comparison of fast (5 participants) and moderate (10 participants) progressors. The model in equati 3 was re-estimated within both groups.

We fit a separate model for HC participants, as they did not complete the ALSFRS-R. To avoid undue influence of individuals with an unusually high number of visits (Fig. A1), we excluded any visits occurring over 2 years (730 days) post-enrollment. Time in study was considered as a predictor but was found to be insignificant based on a LRT. Therefore, we adopted the following model for HC participants:

$$A_{ij} = \beta_0 + b_{0i} + \beta_1 age_i + \beta_2 sex_i + \epsilon_{ij}, \quad \epsilon_{ij} \sim N\left(0, \sigma^2\right). \tag{4}$$

where β_0 represents the mean size of activation across HC participants and b_{0i} represents the random deviation for participant i. The models in equations (2) to (4) were fit in R using the lmer function from the lme4 package, version 1.1–23 (Bates et al., 2015).

3. Results

We first assessed the reliability of the areas of activation produced by the longitudinal spatial Bayesian GLM in healthy controls, compared with the classical GLM. See Supplementary Section E for details. We observed that the Bayesian GLM produced noticeably smoother estimates and much larger areas of activation at a given effect size, while maintaining FWER control. We also analyzed the longitudinal stability of HC participants' areas of activation, which should not change substantially over time, and found that the Bayesian GLM produced more stable results. For the subsequent analysis, we therefore adopted the Bayesian GLM.

Fig. 2 displays longitudinal estimates and areas of activation for one HC and ALS participant. In the HC participant, the area of peak contralateral activation intensity was fairly consistent across visits. However, in the ALS participant, the peak intensified from visits 4 to 5 then shrunk markedly from visits 5 to 6. These patterns are reflected by the areas of activation, particularly $>1\%$ or $>2\%$ signal change. Similar patterns of increasing-then-decreasing activation over time were observed consistently in ALS participants. The participant shown, A26, was observed in Fig. 1 to show a rapid functional decline over their final three visits (the ones displayed in Fig. 2). We next examined this non-linear relationship between functional disability in ALS and size of motor activation.

Fig. 3 displays coefficient curves for the random intercept model given in Eqn. 2 relating *Total Disability* in ALS to size of activation during right hand clenching. Each line represents the estimated relationship between disability and size of contralateral or ipsilateral activation at a given effect size. The colored dots on the left represent the corresponding mean activation in HCs, based on the model in Eqn. 4. The relationship is decreasing overall, but with marked non-linear features, most notably an increase in size of activation at moderate levels of disability. This suggests two distinct phenomena: a period of hyper-activation accompanied by an overall long-term decline in size of activation. To better understand the drivers of these two distinct abnormal activation patterns, we then concurrently examined the relationship between size of activation and two separate measures of disability: *Hand Motor Disability* and *Other Disability*.

Fig. 4 displays coefficient curves estimating the relationship between size of activation and these two separate disability measures, based on the random intercept model given in Eqn. 3. Each line represents the estimated relationship between the predictor shown on the x-axis and size of activation at a given effect size, holding the other predictor constant at zero. The relationship between size of activation and *Hand Motor Disability* exhibits a clear inverted U-shaped relationship: at moderate levels of disability, there is a sharp increase over the normal size of activation in HCs, but with further disability there is a rapid decline to abnormally low levels. Considering only measures of disability not associated with hand function (*Other Disability*), there is a purely declining relationship between disability and size of activation. This suggests that hyper-activation during hand clenching is specifically associated with declining hand motor function.

Fig. 4 shows two additional effects. First, the size of activation when *Hand Motor Disability* or *Other Disability* reach higher levels is nearly zero at effect sizes of 1% and 2% in both hemispheres, suggesting near complete loss of neuronal activation as the processes of neurodegeneration associated with ALS disease progression continues. Second, ALS participants with very low levels of disability (*Hand Motor Disability* and *Other Disability* both equalling 0) exhibited slightly elevated contralateral and ipsilateral activation at effect sizes of 1% and 2%, relative to HCs. This suggests that patterns of hyper-activation may occur very early in the ALS disease process, even prior to the onset of measurable disability.

Fig. 5 displays results stratified by progression rate. The overall relationships with *Hand Motor Disability* are consistent with the inverted U-shaped trajectories observed in Fig. 4. However, compared with moderate progressors, fast progressors exhibit three noteworthy differences: first, they tend to have greater baseline size of activation (when *Hand Motor Disability* is near zero); second, they tend to peak higher; third, for 0% effect size, they tend to peak at an milder level of *Hand Motor Disability*. Corresponding plots for ipsilateral activation show similar patterns (see Supplementary Sec. F). Supplementary Fig. F12 displays the relationship between size of activation and *Other Disability* for fast and moderate progressors. Fast progressors also exhibit greater enlargement of activation at low levels of *Other Disability* and decline faster as a function of disability. Since fast progressors experience a given level of disability earlier following symptom onset, these findings suggest that the neuronal manifestations of fast-progressing disability may outpace or even precede clinical disability.

4. Discussion

Using a rich longitudinal task fMRI dataset and an advanced cortical surface spatial Bayesian modeling approach, in this study we observed complex longitudinal trajectories of neurodegeneration related to disability in ALS. Below, we discuss these findings in the context of previous literature and suggest directions for future research into neurodegeneration in ALS. We also discuss the importance of analysis and processing choices for longitudinal modeling and other settings where accurate individual-level brain measures are needed, including biomarker discovery. Finally, we note several limitations of this study.

4.1. Complex trajectories of motor activation

We observed three consistent patterns of change in motor activations. First, we observed increased motor activation elicited by a simple hand clench task associated with mild hand motor disability. Second, as patients experience further disability, we observed a sharp reduction in the size of activation. Third, we also observed reduced activation associated with other aspects of disability. These latter two observations suggest major neuronal degeneration at more advanced levels of disability.

These effects are most clearly observed contralaterally, but ipsilateral activations exhibit similar patterns through the disease process. Note that some level of ipsilateral activation is expected in lateral motor tasks (Konrad et al., 2002), as we observe in HCs and in ALS subjects with very low levels of disability.

We also observed that, compared with moderate progressors, fast progressors had increased hyper-activation occurring at an earlier stage of hand motor disability. These findings indicate that certain patterns of neurodegeneration may precede or outpace the rate of clinical disability. This builds on the finding of Douaud et al. (2011), who observed differential functional connectivity patterns in ALS, in which individuals with slower progression rates more closely resembled HCs.

These findings substantially advance prior understanding of motor neurodegeneration in ALS. Such discoveries were made possible by our rich longitudinal study that followed ALS participants over the course of disease progression, from mild to more advanced disability. Following participants until they were no longer able to undergo scanning enabled us to discover a late decline in activation following the initial increase associated with milder disability. While increased motor activation in ALS has been noted in previous studies (Konrad et al., 2002; Poujois et al., 2013; Schoenfeld et al., 2005), to our knowledge this subsequent decline has not been observed in prior literature. This, along with the decline we observed associated with non-hand disability, likely reflects the drastic motor neuron loss known to occur in ALS (Subramaniam, 2019).

4.2. Does increased activation reflect compensation or loss of inhibition?

Our observation of increased motor activation associated with mild hand disability is consistent with several studies over the past two decades using fMRI to reveal motor cortex changes in ALS. However, we observe more complex longitudinal trajectories, which

suggest that the initial hyper-activation may not be fully attributable to compensation, as suggested by earlier work. Previously, Konrad et al. (2002), Schoenfeld et al. (2005) and Poujois et al. (2013) observed enlarged activations during motor tasks. Poujois et al. (2013) related this to disease progression rate but with cross-sectional data. Such hyper-activation has been typically interpreted as a *compensatory* process enabling the patient to complete the task in ALS (Konrad et al., 2002; Schoenfeld et al., 2005), building from findings in healthy aging (Fitzhugh et al., 2019; Park et al., 2003). In ALS, however, increased activation could alternatively be attributed to *diminished inhibitory signaling* within the brain (Poujois et al., 2013), which is known to occur in ALS.

Our findings point to loss of inhibition as a likely contributor to the hyper-activation associated with mild disability. First, we observe similar patterns of early hyper-activation *ipsilaterally*, which is more suggestive of loss of inhibition. Second and perhaps more notably, the differential trajectories observed across fast and moderate progressors conflict with a pure compensation model, since these two groups are experiencing hyper-activation at different levels of motor ability. Instead, through the lens of loss of inhibition, the earlier and more extreme hyper-activation observed in fast progressors may simply reflect more extreme and rapid neurodegeneration of inhibitory pathways at this stage of the disease process in fast progressors. It is possible that such an initial loss of inhibition, followed by later hypo-activation with additional disease burden, are part of a single process of motor neuron loss in ALS (Subramaniam, 2019).

Prior studies employing other neuroimaging modalities can also shed light on this question. Transcranial magnetic stimulation (TMS) has been used to probe inter-hemispheric communication, specifically early intracortical inhibition (ICI). (Zanette et al., 2002) observed that abnormal ICI developed early in the ALS disease process and continued to further degrade with disease progression. Magnetic resonance spectroscopy (MRS) has revealed decreased endogenous gamma-Aminobutyric acid (GABA) (Foerster et al., 2013; Lloyd et al., 2000), a principal inhibitory neurotransmitter, in individuals with ALS. Although another study of GABA by Blicher et al. (2019) did not see such a change, it was based on a small sample and voxel size, which may have led to insufficient statistical power. Studies of functional connectivity have produced somewhat conflicting findings, reporting both increased and decreased connectivity (Jelsone-Swain et al., 2010; Mohammadi et al., 2009; Verstraete et al., 2010). Douaud et al. (2011) suggested a possible explanation for this. Using functional and structural connectivity, they observed initial loss of inter-hemispheric inhibition giving rise to increased trans-hemispheric connectivity. This eventually wanes due to loss of the neurons responsible for the random fluctuations producing functional connectivity, with connectivity greatly diminishing and eventually falling below baseline as the patient progresses. This is consistent with our findings of an inverted U-shaped activation trajectory. In sum, there is strong prior evidence for loss of inhibition in ALS from studies employing TMS, MRS, and connectivity.

4.3. Producing accurate individual-level measures of brain function

Our discoveries were facilitated by a sophisticated analysis approach designed to provide accurate and reliable individual-level measures of task activation, in contrast with

conventional task fMRI analysis methods that tend to exhibit poor reliability in individuals (Elliott et al., 2020). This is important for longitudinal studies, as well as other settings where robust and reliable individual-level measures are needed. Two key aspects of our approach were: 1) performing analysis in subject-specific surface space and 2) adopting a novel longitudinal surface-based spatial Bayesian GLM.

4.3.1. Performing analysis in subject surface space—We constructed subject-specific surface templates, enabling us to preserve anatomical features and avoid potential normalization issues in individuals with neurodegenerative disease. Eloyan et al. (2014) gave a striking example of such issues in multiple sclerosis: they found that standard normalization methods resulted in a large proportion of white matter lesions being relocated outside of white matter. Even if subjects are aligned anatomically, they may not align functionally due to individual differences, reducing the utility of voxel-level comparisons in standard space (Dubois and Adolphs, 2016). Issues of misalignment and distortion can be mitigated by performing analyses in subject space. Performing surface-based analysis also helped enhance specificity by avoiding blurring across tissue classes or distinct areas of the cortex (Brodoehl et al., 2020).

Subject-space analyses require aggregating and comparing subject-level results in a different way than traditional voxel-wise comparisons. In our analysis, we used size of activation as the basis for examining disease trajectories and group differences, facilitated by the robust areas of activation produced by the spatial Bayesian GLM. Several alternatives are possible: Gupta et al. (2010) used spatial properties of activation patterns for predictive modeling, while Stern et al. (2009) used topographical analysis. Both approaches outperformed voxel-wise group-difference analysis in terms of discovering disease effects. Notably, Stern et al. (2009) found HCs to exhibit high spatial heterogeneity in activation, suggesting that performing analysis in subject space may be beneficial more generally.

4.3.2. The advantages of longitudinal spatial bayesian modeling—Surface-based spatial Bayesian modeling of task activation has been previously validated and shown to produce more accurate and robust activations by leveraging spatial dependencies (Mejia et al., 2020). We proposed a novel longitudinal extension, which we validated by examining the stability of results for HC participants over time (see Supplementary Section E). This extension has important advantages over the single-session model. By pooling information across sessions to estimate model parameters, it produces more accurate estimates and areas of activation and reduces longitudinal noise, enhancing subsequent longitudinal analysis. This modeling framework can be extended to non-longitudinal contexts, such as cross-sectional studies with multiple sessions per subject or small group studies.

4.4. The next frontier: Biomarker discovery

Motor cortex changes hold potential as a possible biomarker for ALS disease diagnosis and progression. Brain signatures may signal early loss of inhibition, even in pre-symptomatic disease, that might serve as a biomarker for ALS diagnosis. Changes (structural and functional connectivity) due to the ALS disease process (Lee et al., 2017) have been observed in pre-symptomatic carriers of C9orf72 (a genetic defect linked to ALS (Renton

et al., 2011). Our findings suggest the possibility of very early hyper-activation above a scientifically meaningful effect size. Future work should assess hyper-activation and loss of inhibition as potential biomarkers for pre-clinical ALS. Declining motor activation following a period of over-activation may also serve as a marker of a change to a later phase of disease progression.

Clinical trials employing clinical outcome measures are typically lengthy and expensive. Development of a brain biomarker of ALS reflecting enhanced understanding of pathophysiology would have major implications for clinical trials and therapies (Gordon et al., 2010) by making them more efficient and effective (Turner et al., 2013). For example, a trial of a drug targeting abnormal cortical excitability could employ such a biomarker to select only subjects that are in early phases of motor neurodegeneration. Perhaps more importantly, such a biomarker could also be used to monitor and guide treatment, by escalating drug dosage until suppression of hyper-excitability is achieved or decline in activation over time is arrested. Vitally, a biomarker that is sensitive to cortical changes could produce evidence of drug intervention efficacy prior to manifestation in measurable clinical decline (Turner et al., 2009).

4.5. Study limitations

As with other rare neurological diseases, neuroimaging studies of ALS are difficult to execute. Given the rarity and typically short survival time characterizing ALS, sample sizes tend to be smaller, especially for single-site studies. While consortia studies are taking place, these are currently focused on structural and resting state investigation (Bharti et al., 2020). While the sample size in our study is a limitation, a literature search suggests that our study is one of the largest, if not the largest (Castelnovo et al., 2020; Trojsi et al., 2020), longitudinal studies investigating BOLD activation in ALS. We sought to mitigate the negative impacts of small sample size by employing a sophisticated analysis approach, thus avoiding the power issues associated with a classical massive univariate analysis.

Three additional limitations of our sample are important to note. First, three of our ALS subjects were enrolled over 4 years since first symptom onset. However, these were otherwise not unusual in terms of overall disease progression rate or disability levels during their scanning sessions. Since disease progression in ALS is highly heterogeneous and we used disability and disease progression rates as predictors rather than time since symptom onset, we elected to include these subjects in our analysis. Second, while four ALS participants had CBS scores indicating possible frontotemporal dementia (FTD), three of the four were close to the cutoff for FTD. Future work should focus on collecting larger longitudinal neuroimaging studies of ALS, including consortia studies, to increase sample sizes and make it possible to investigate possible interactions between ALS and FTD. Third, we did not test for C9orf72 repeat expansion, since unfortunately this genetic test was not widely available at the time of data collection.

One limitation common to neuroimaging studies of ALS is the requirement that ALS participants must be capable of lying in a supine position for some length of time during MRI scanning. While this constraint can be lessened by allowing the individual to take breaks and sit up as needed, it still imposes a bias on neuroimaging studies of ALS (van der

Burgh et al., 2020), since they are limited to only those that can tolerate the MRI. A seated-position MRI would allow patients with more disability to participate, but these systems have greatly reduced magnetic field strengths of 0.25T (G-scan; Esaote SpA, Genoa, Italy) or 0.60T (FONAR Melville, New York, USA). To mitigate this source of bias, we examine cortical activation as a function of physical disability, as opposed to time since symptom onset, which helps account for the bias toward subjects with lower disease burden. Even so, our study is limited in terms of the range of disease severity we were able to observe.

In our analysis, we only considered activation within the motor mask (Supplementary Fig. C4), so activation in other areas cannot be observed. It is conceivable that the enlarged areas of activation we observe in ALS may expand beyond the mask used in this study, resulting in possible underestimation of size of activation for some subjects. Additionally, our analysis did not include subcortical or cerebellar areas. Future work should focus on analyzing longitudinal trajectories of motor activation in ALS across the entire cortex and within relevant subcortical and cerebellar regions. Our analysis also did not consider atrophy over the course of ALS disease progression. Atrophy may help to partly explain the dramatic drop in motor activation occurring with high disability but would not explain increased activation at lower levels of disability. Future research should aim to development models to incorporate atrophy.

Finally, we employed a two-stage statistical approach: in the first stage we fit a longitudinal spatial Bayesian GLM on the data from each participant, based on which we estimated the size of activation at each visit; in the second stage we fit a series of group-level linear mixed-effects models, where we studied the relationship between size of activation and disease progression. Besides computational considerations, in our analysis there are two other reasons to employ a two-stage approach. First, the unit of analysis in our second-stage mixed effects models is the entire brain, rather than individual vertices, so designing a hierarchical model to identify the group-level covariate effects of interest would not be trivial. Second, we performed all analyses in subjects' native space to preserve the unique cortical anatomy of each participant. This is particularly important here because of the negative impacts of neurodegeneration on inter-subject registration. Therefore, subjects are not spatially aligned and cannot be jointly analyzed vertex-wise in a single hierarchical model. We note that our two-stage approach is analogous to traditional two-stage modeling in task fMRI, where subject-level estimates produced at the first-level GLM become the response variable in a second-level group model (Holmes, 1988). Mumford and Nichols (2009) showed that this approach produces unbiased second-level coefficient estimates, which are also efficient if errors are homogeneous at the first level. This is because the estimation error of first-level effects is absorbed into the error variance in the second-level model. In the same way, our linear mixed-effects models account for estimation error in the size of activation produced from the spatial Bayesian GLMs and therefore should produce unbiased estimates of group-level covariate effects. If we assume homogeneous error variance in the size of activation estimates across subjects, then our covariate effect estimates will also be efficient. Future research should focus on formally quantifying and accounting for uncertainty in second-level analysis of the size of activation produced from first-level GLMs, particularly in the case of heterogeneous errors.

5. Conclusion

In this paper, we adopted a sophisticated longitudinal surface-based Bayesian analysis approach to analyze a rich longitudinal fMRI study of ALS. In this study, individuals with ALS and matched healthy controls were observed regularly for 1–2 years or longer. Our analyses revealed a complex trajectory of cortical activation during a simple motor hand clench task: activation initially spreads within contralateral and ipsilateral motor areas, but with additional disease burden activations sharply diminish and eventually nearly disappear. We observed systematic differences based on clinical progression rate, with fast progressors exhibiting more extreme effects earlier in the disease process. The nuances of these findings suggest that initial hyper-activation—observed in earlier studies but assumed to be due to functional compensation—is likely due to a loss of inhibitory signals forming part of a larger process of neuronal decay and death. These discoveries were made possible by pairing a rich longitudinal fMRI dataset with a surface-based spatial Bayesian modeling approach capable of identifying activations in individuals over time with high accuracy and power. Our study establishes that this advanced statistical approach furthers the study of neurodegenerative disease and is promising for the study of other time-varying processes such as development and aging. The surface-based spatial Bayesian GLM is implemented in a user-friendly R package, BayesfMRI.

Supplementary Material

Refer to Web version on PubMed Central for supplementary material.

Acknowledgments

This study would not have been possible without the generous commitment of our participants with amyotrophic lateral sclerosis and their families. These patients and their families committed years to this study during an exceedingly difficult time in their lives, especially true for a longitudinal study such as ours. This work is dedicated to these patients.

Funding

This work was supported by the National Institute of Biomedical Imaging and Bioengineering at the National Institutes of Health (R01EB027119 to A.F.M.), the National Institute of Neurological Disorders and Stroke at the National Institutes of Health (R01NS052514, R01NS082304 to R.C.W.), and the Department of Radiology at the University of Michigan (BRS Award to R.C.W).

References

Agosta F, Valsasina P, Riva N, Copetti M, Messina MJ, Prelle A, Comi G, Filippi M, 2012. The cortical signature of amyotrophic lateral sclerosis. PLoS ONE 7 (8), e42816.

Akaike H, 1998. Information Theory and an Extension of the Maximum Likelihood Principle. In: Selected papers of Hirotugu Akaike. Springer, pp. 199–213.

Avants BB, Tustison NJ, Song G, Cook PA, Klein A, Gee JC, 2011. A reproducible evaluation of ANTs similarity metric performance in brain image registration. Neuroimage 54 (3), 2033–2044. [PubMed: 20851191]

Bates D, Mächler M, Bolker B, Walker S, 2015. Fitting linear mixed-effects models using lme4. J. Stat. Softw 67 (1), 1–48. doi: 10.18637/jss.v067.i01.

Benjamini Y, Hochberg Y, 1995. Controlling the false discovery rate: a practical and powerful approach to multiple testing. J. R. Stat. Soc.: Ser. B (Stat. Methodol.) 289–300.

Bharti K, Khan M, Beaulieu C, Graham SJ, Briemberg H, Frayne R, Genge A, Korngut L, Zinman L, Kalra S, Consortium, f.t.C.A.N., 2020. Involvement of the dentate nucleus in the pathophysiology of amyotrophic lateral sclerosis: a multi-center and multi-modal neuroimaging study. Neuroimage: Clinical 28, 102385.

Blicher JU, Eskildsen SF, rmose T.G.S.x., ller A.T.M.x., Figlewski K, Near J, 2019. Short echo-time magnetic resonance spectroscopy in ALS, simultaneous quantification of glutamate and GABA at 3T. Sci. Rep 1–7. [PubMed: 30626917]

Brodoehl S, Gaser C, Dahnke R, Witte OW, Klingner CM, 2020. Surface-based analysis increases the specificity of cortical activation patterns and connectivity results. Sci. Rep 10 (1), 1–13. [PubMed: 31913322]

Brooks BR, 1994. El Escorial World Federation of Neurology criteria for the diagnosis of amyotrophic lateral sclerosis. Subcommittee on Motor Neuron Diseases/Amyotrophic Lateral Sclerosis of the World Federation of Neurology Research Group on Neuromuscular Diseases and the El Escorial "Clinical limits of amyotrophic lateral sclerosis " workshop contributors. J. Neurol. Sci 124, 96. [PubMed: 7807156]

van der Burgh HK, Westeneng H-J, Walhout R, van Veenhuijzen K, Tan HHG, Meier JM, Bakker LA, Hendrikse J, van Es MA, Veldink JH, Van Den Heuvel MP, van den Berg LH, 2020. Multimodal longitudinal study of structural brain involvement in amyotrophic lateral sclerosis. Neurology 94 (24), e2592–e2604. [PubMed: 32414878]

Castelnovo V, Canu E, Calderaro D, Riva N, Poletti B, Basaia S, Solca F, Silani V, Filippi M, Agosta F, 2020. Progression of brain functional connectivity and frontal cognitive dysfunction in ALS. YNICL 28, 102509.

Chapman MC, Jelsone-Swain L, Johnson TD, Gruis KL, Welsh RC, 2014. Diffusion tensor MRI of the corpus callosum in amyotrophic lateral sclerosis. J. Magn. Reson. Imaging 39 (3), 641–647. [PubMed: 23843179]

Cremers HR, Wager TD, Yarkoni T, 2017. The relation between statistical power and inference in fMRI. PLoS ONE 12 (11), e0184923.

Douaud G, Filippini N, Knight S, Talbot K, Turner MR, 2011. Integration of structural and functional magnetic resonance imaging in amyotrophic lateral sclerosis. Brain 134 (Pt 12), 3470–3479. [PubMed: 22075069]

Dubois J, Adolphs R, 2016. Building a science of individual differences from fMRI. Trends Cogn. Sci. (Regul. Ed.) 20 (6), 425–443.

Elliott ML, Knodt AR, Ireland D, Morris ML, Poulton R, Ramrakha S, Sison ML, Moffitt TE, Caspi A, Hariri AR, 2020. What is the test-retest reliability of common task-fMRI measures? New empirical evidence and a meta-analysis. Psychological Science 31 (7), 792–806. [PubMed: 32489141]

Ellis CM, Simmons A, Jones D, Bland J, Dawson JM, Horsfield M, Williams SC, Leigh PN, 1999. Diffusion tensor MRI assesses corticospinal tract damage in ALS. Neurology 53 (5), 1051–1058. [PubMed: 10496265]

Eloyan A, Shou H, Shinohara RT, Sweeney EM, Nebel MB, Cuzzocreo JL, Calabresi PA, Reich DS, Lindquist MA, Crainiceanu CM, 2014. Health effects of lesion localization in multiple sclerosis: spatial registration and confounding adjustment. PLoS ONE 9 (9), e107263.

Fischl B, 2012. Freesurfer. Neuroimage 62 (2), 774–781. [PubMed: 22248573]

Fitzhugh MC, Braden BB, Sabbagh MN, Rogalsky C, Baxter LC, 2019. Age-related atrophy and compensatory neural networks in reading comprehension. J. Int. Neuropsychol. Soc 25 (6), 569–582. [PubMed: 31030698]

Foerster BR, Pomper MG, Callaghan BC, Petrou M, Edden RAE, Mohamed MA, Welsh RC, Carlos RC, Barker PB, Feldman EL, 2013. An imbalance between excitatory and inhibitory neurotransmitters in amyotrophic lateral sclerosis revealed by use of 3-T proton magnetic resonance spectroscopy. JAMA Neurol. 70 (8), 1009–1016. [PubMed: 23797905]

Friston K, Ashburner J, Kiebel S, Nichols T, Penny W.(Eds.), 2007. Statistical parametric mapping: The analysis of functional brain images. Academic Press.

Friston K, Penny W, 2003. Posterior probability maps and spms. Neuroimage 19 (3), 1240–1249. [PubMed: 12880849]

Gordon PH, Cheng B, Salachas F, Pradat P-F, Bruneteau G, Corcia P, Lacomblez L, Meininger V, 2010. Progression in ALS is not linear but is curvilinear. J. Neurol 257 (10), 1713–1717. [PubMed: 20532545]

Gray KR, Wolz R, Heckemann RA, Aljabar P, Hammers A, Rueckert D, Alzheimer's Disease Neuroimaging Initiative, 2012. Multi-region analysis of longitudinal FDG-PET for the classification of Alzheimer's disease. Neuroimage 60 (1), 221–229. [PubMed: 22236449]

Gupta L, Besseling RMH, Overvliet GM, Hofman PAM, de Louw A, Vaessen MJ, Aldenkamp AP, Ulman S, Jansen JFA, Backes WH, 2010. Spatial heterogeneity analysis of brain activation in fMRI. Neuroimage: Clinical 5, 266–276.

Holmes A, 1988. Generalisability, random effects and population inference. Neuroimage 7.

Jelsone-Swain LM, Fling BW, Seidler RD, Hovatter R, Gruis K, Welsh RC, 2010. Reduced interhemispheric functional connectivity in the motor cortex during rest in limb-onset amyotrophic lateral sclerosis. Front. Syst. Neurosci 4, 158. [PubMed: 21228916]

Kassubek J, Muller HP, Del Tredici K, Brettschneider J, Pinkhardt EH, Lule D, Bohm S, Braak H, Ludolph AC, 2014. Diffusion tensor imaging analysis of sequential spreading of disease in amyotrophic lateral sclerosis confirms patterns of TDP-43 pathology. Brain 137 (6), 1733–1740. [PubMed: 24736303]

Kolinger GD, Vállez García D, Willemsen ATM, Reesink FE, de Jong BM, Dierckx RAJO, De Deyn PP, Boellaard R, 2021. Amyloid burden quantification depends on PET and MR image processing methodology. PLoS ONE 16 (3), e0248122.

Konrad C, Henningsen H, Bremer J, Mock B, Deppe M, Buchinger C, Turski P, Knecht S, Brooks B, 2002. Pattern of cortical reorganization in amyotrophic lateral sclerosis: a functional magnetic resonance imaging study. Exp. Brain Res 143 (1), 51–56. [PubMed: 11907690]

Konrad C, Jansen A, Henningsen H, Sommer J, Turski PA, Brooks BR, Knecht S, 2006. Subcortical reorganization in amyotrophic lateral sclerosis. Exp. Brain Res. Exp. Hirnforschung Expérimentation cérébrale 172 (3), 361–369.

Lawrence E, Vegvari C, Ower A, Hadjichrysanthou C, De Wolf F, Anderson RM, 2017. A systematic review of longitudinal studies which measure Alzheimer's disease biomarkers. J. Alzheimers Dis 59 (4), 1359–1379. [PubMed: 28759968]

Lee SE, Sias AC, Mandelli ML, Brown JA, Brown AB, Khazenzon AM, Vidovszky AA, Zanto TP, Karydas AM, Pribadi M, Dokuru D, Coppola G, Geschwind DH, Rademakers R, Gorno-Tempini ML, Rosen HJ, Miller BL, Seeley WW, 2017. Network degeneration and dysfunction in presymptomatic C9ORF72 expansion carriers. Neuroimage: Clinical 14, 286–297. [PubMed: 28337409]

Liu TT, Frank LR, Wong EC, Buxton RB, 2001. Detection power, estimation efficiency, and predictability in event-related fMRI. Neuroimage 13 (4), 759–773. [PubMed: 11305903]

Lloyd CM, Richardson MP, Brooks DJ, Al-Chalabi A, Leigh PN, 2000. Extramotor involvement in ALS: PET studies with the GABA(a) ligand [(11)C]flumazenil. Brain 123 (Pt 11), 2289–2296. [PubMed: 11050028]

Mejia AF, Nebel MB, Eloyan A, Caffo B, Lindquist MA, 2017. PCA Leverage: outlier detection for high-dimensional functional magnetic resonance imaging data. Biostatistics 18 (3), 521–536. [PubMed: 28334131]

Mejia AF, Yue Y, Bolin D, Lindgren F, Lindquist MA, 2020. A Bayesian general linear modeling approach to cortical surface fMRI data analysis. J. Am. Stat. Assoc 115 (530), 501–520. [PubMed: 33060871]

Menke RAL, Abraham I, Thiel CS, Filippini N, Knight S, Talbot K, Turner MR, 2012. Fractional anisotropy in the posterior limb of the internal capsule and prognosis in amyotrophic lateral sclerosis : fractional anisotropy and ALS. Arch. Neurol 69 (11), 1493. [PubMed: 22910997]

Menke RAL, Proudfoot M, Talbot K, Turner MR, 2018. The two-year progression of structural and functional cerebral MRI in amyotrophic lateral sclerosis. Neuroimage: Clinical 17, 953–961. [PubMed: 29321969]

Mohammadi B, Kollewe K, Samii A, Krampfl K, Dengler R, Münte TF, 2009. Changes of resting state brain networks in amyotrophic lateral sclerosis. Exp. Neurol 217 (1), 147–153. [PubMed: 19416664]

Monti MM, 2011. Statistical analysis of fMRI time-series: a critical review of the GLM approach. Front. Hum. Neurosci 5, 28. [PubMed: 21442013]

Müller H-P, Turner MR, Grosskreutz J, Abrahams S, Bede P, Govind V, Prudlo J, Ludolph AC, Filippi M, Kassubek J, 2016. A large-scale multicentre cerebral diffusion tensor imaging study in amyotrophic lateral sclerosis. J. Neurol. Neurosurg. Psychiatry 87 (6), 570–579. [PubMed: 26746186]

Mumford JA, Nichols T, 2009. Simple group fMRI modeling and inference. Neuroimage 47 (4), 1469–1475. [PubMed: 19463958]

Murdock BJ, Famie JP, Piecuch CE, Raue KD, Mendelson FE, Pieroni CH, Iniguez SD, Zhao L, Goutman SA, Feldman EL, 2021. Nk cells associate with als in a sex-and age-dependent manner. JCI Insight 6 (11).

Noll D, 2002. Rapid MR image acquisition in the presence of background gradients. Proc. IEEE Int. Sympos. Biomed. Imag 725–728.

Noll DC, Meyer CH, Pauly JM, Nishimura DG, Macovski A, 2004. A homogeneity correction method for magnetic resonance imaging with time-varying gradients. IEEE Trans. Med. Imag 10 (4), 629–637.

Park DC, Welsh RC, Marshuetz C, Gutchess AH, Mikels J, Polk TA, Noll DC, Taylor SF, 2003. Working memory for complex scenes: age differences in frontal and hippocampal activations. J. Cogn. Neurosci 15 (8), 1122–1134. [PubMed: 14709231]

Poujois A, Schneider FC, Faillenot I, Camdessanché J-P, Vandenberghe N, Thomas-Antérion C, Antoine J-C, 2013. Brain plasticity in the motor network is correlated with disease progression in amyotrophic lateral sclerosis. Hum. Brain Mapp 34 (10), 2391–2401. [PubMed: 22461315]

Renton AE, Majounie E, Waite A, Simón-Sánchez J, Rollinson S, Gibbs JR, Schymick JC, Laaksovirta H, van Swieten JC, Myllykangas L, Kalimo H, Paetau A, Abramzon Y, Remes AM, Kaganovich A, Scholz SW, Duckworth J, Ding J, Harmer DW, Hernandez DG, Johnson JO, Mok K, Ryten M, Trabzuni D, Guerreiro RJ, Orrell RW, Neal J, Murray A, Pearson J, Jansen IE, Sondervan D, Seelaar H, Blake D, Young K, Halliwell N, Callister JB, Toulson G, Richardson A, Gerhard A, Snowden J, Mann D, Neary D, Nalls MA, Peuralinna T, Jansson L, Isoviita V-M, Kaivorinne A-L, Hölttä-Vuori M, Ikonen E, Sulkava R, Benatar M, Wuu J, Chiò A, Restagno G, Borghero G, Sabatelli M, Heckerman D, Rogaeva E, Zinman L, Rothstein JD, Sendtner M, Drepper C, Eichler EE, Alkan C, Abdullaev Z, Pack SD, Dutra A, Pak E, Hardy J, Singleton A, Williams NM, Heutink P, Pickering-Brown S, Morris HR, Tienari PJ, Traynor BJ, Consortium28, T.I., 2011. A hexanucleotide repeat expansion in C9ORF72 is the cause of chromosome 9p21-Linked ALS-FTD. Neuron 72 (2), 257–268. [PubMed: 21944779]

Rooney J, Burke T, Vajda A, Heverin M, Hardiman O, 2017. What does the ALSFRS-R really measure? A longitudinal and survival analysis of functional dimension subscores in amyotrophic lateral sclerosis. J. Neurol. Neurosurg. Psychiatry 88 (5), 381–385. [PubMed: 27888187]

Schoenfeld MA, Tempelmann C, Gaul C, Kühnel GR, Düzel E, Hopf J-M, Feistner H, Zierz S, Heinze HJ, Vielhaber S, 2005. Functional motor compensation in amyotrophic lateral sclerosis. J. Neurol 252 (8), 944–952. [PubMed: 15750701]

Shan ZY, Wright MJ, Thompson PM, McMahon KL, Blokland GGAM, de Zubicaray GI, Martin NG, Vinkhuyzen AAE, Reutens DC, 2013. Modeling of the hemodynamic responses in block design fMRI studies. J. Cerebral Blood Flow Metabol 34 (2), 316–324.

Stern ER, Welsh RC, Fitzgerald KD, Taylor SF, 2009. Topographic analysis of individual activation patterns in medial frontal cortex in schizophrenia. Hum. Brain Mapp 30 (7), 2146–2156. [PubMed: 18819107]

Stoppel CM, Vielhaber S, Eckart C, Machts J, Kaufmann J, Heinze H-J, Kollewe K, Petri S, Dengler R, Hopf J-M, Schoenfeld MA, 2014. Structural and functional hallmarks of amyotrophic lateral sclerosis progression in motor-and memory-related brain regions. Neuroimage: Clinical 5, 277–290. [PubMed: 25161894]

Subramaniam S, 2019. Selective neuronal death in neurodegenerative diseases: the ongoing mystery. Yale J. Biol. Med 92 (4), 695–705. [PubMed: 31866784]

Telzer EH, McCormick EM, Peters S, Cosme D, Pfeifer JH, van Duijvenvoorde AC, 2018. Methodological considerations for developmental longitudinal fMRI research. Dev. Cogn. Neurosci 33, 149–160. [PubMed: 29456104]

Trojsi F, Di Nardo F, Siciliano M, Caiazzo G, Femiano C, Passaniti C, Ricciardi D, Russo A, Bisecco A, Esposito S, Monsurrò MR, Cirillo M, Santangelo G, Esposito F, Tedeschi G, 2020. Frontotemporal degeneration in amyotrophic lateral sclerosis (ALS): a longitudinal MRI one-year study. CNS Spectr. 1–10.

Turner MR, Hardiman PO, Benatar M, Brooks BR, Chiò A, de Carvalho MD M, Ince PG, Lin C, Miller RG, Mitsumoto H, Nicholson G, Ravits J, Shaw PJ, Swash M, Talbot K, Traynor BJ, van den Berg LH, Veldink JH, Vucic S, Kiernan MC, 2013. Controversies and priorities in amyotrophic lateral sclerosis. Lancet Neurol. 12 (3), 310–322. [PubMed: 23415570]

Turner MR, Kiernan MC, Leigh PN, Talbot K, 2009. Biomarkers in amyotrophic lateral sclerosis. Lancet Neurol. 8 (1), 94–109. [PubMed: 19081518]

Turner MR, Modo M, 2010. Advances in the application of MRI to amyotrophic lateral sclerosis. Expert Opin. Med. Diagn 4 (6), 483–496. [PubMed: 21516259]

Verstraete E, Van Den Heuvel MP, Veldink JH, Blanken N, Mandl RC, Hulshoff Pol HE, van den Berg LH, 2010. Motor network degeneration in amyotrophic lateral sclerosis: a structural and functional connectivity study. PLoS ONE 2012 (10), e13664.

Woo C-W, Chang LJ, Lindquist MA, Wager TD, 2017. Building better biomarkers: brain models in translational neuroimaging. Nat. Neurosci 20 (3), 365. [PubMed: 28230847]

Woolrich MW, Jbabdi S, Patenaude B, Chappell M, Makni S, Behrens T, Beckmann C, Jenkinson M, Smith SM, 2009. Bayesian analysis of neuroimaging data in FSL. Neuroimage 45 (1), S173–S186. [PubMed: 19059349]

Worsley KJ, Friston KJ, 1995. Analysis of fMRI time-series revisited - again. Neuroimage 2 (3), 173–181. [PubMed: 9343600]

Zanette G, Tamburin S, Manganotti P, Refatti N, Forgione A, Rizzuto N, 2002. Different mechanisms contribute to motor cortex hyperexcitability in amyotrophic lateral sclerosis. Clin. Neurophysiol 113 (11), 1688–1697. [PubMed: 12417221]

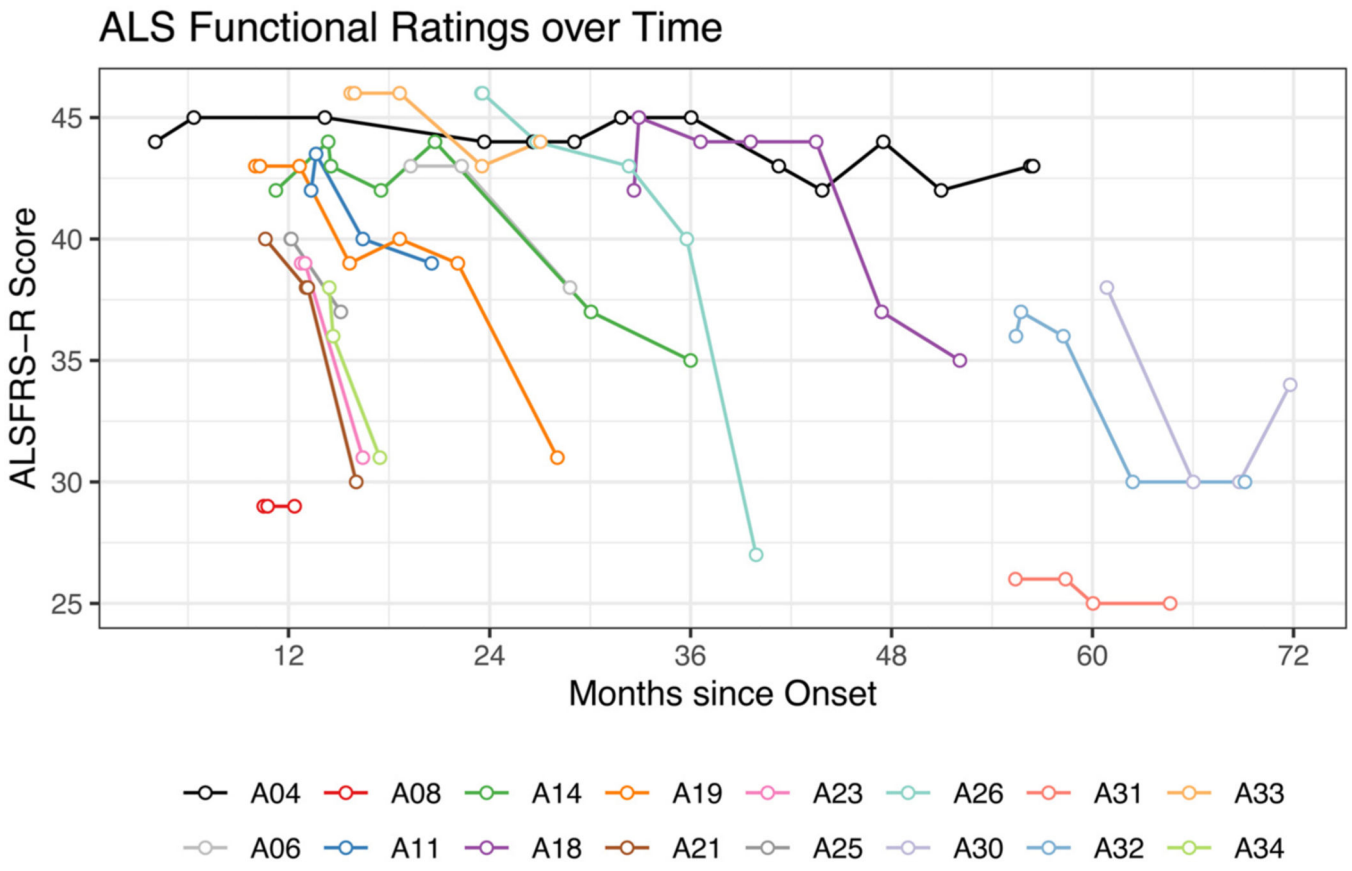

Fig. 1. ALSFRS-R disease trajectories over time.

ALS Functional Rating Scale (revised) (ALSFRS-R) scores range from 48 (no impairment) to 0 (total impairment). Each line represents an individual participant with ALS. Note that for many participants, the first two visits occurred in quick succession and appear over-lapping on the plot. These clinical trajectories illustrate the wide heterogeneity of the disease process, with some patients exhibiting rapid clinical progression (e.g., A08, A21, A23, A25, A34) while others exhibit very slow progression (e.g., A04).

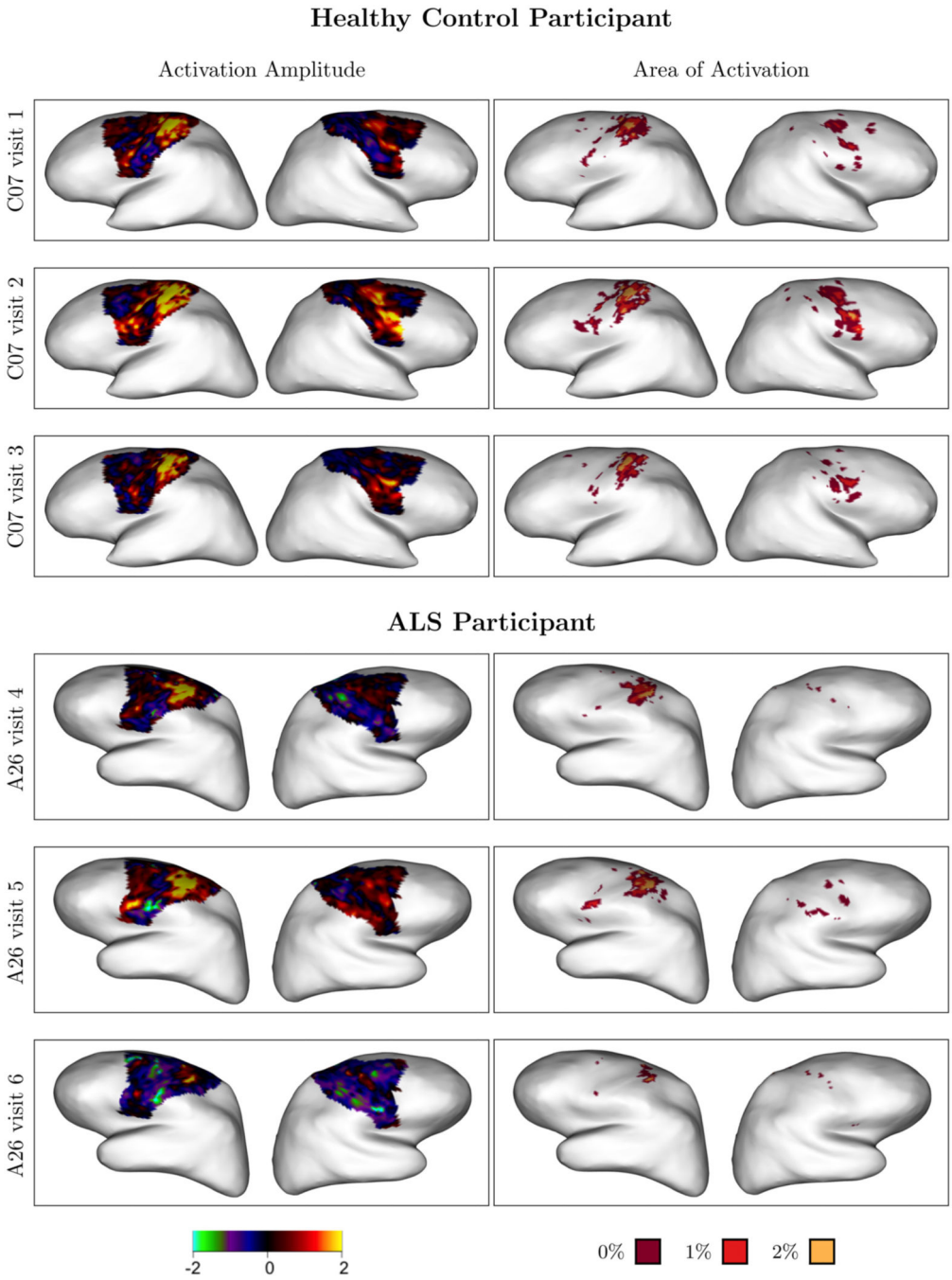

Fig. 2. Estimates and areas of activation during hand clenching in one HC and one ALS participant.

Areas of activation show binary maps of significance at three nested effect sizes, $\gamma = 0\%$ (red plus orange plus yellow), 1% (orange plus yellow), and 2% (yellow). **Top panel:** The HC participant shows relatively stable patterns of activation over time. **Bottom panel:** The ALS participant shows noticeable changes between visits 4, 5 and 6 (their final three visits during the study). Between visits 4 and 5, the size of peak activation appears to increase somewhat, while between visits 5 and 6 the area peak activation virtually disappears.

Similar patterns are observed in other ALS participants and appear to reflect dynamics of neurodegeneration in ALS.

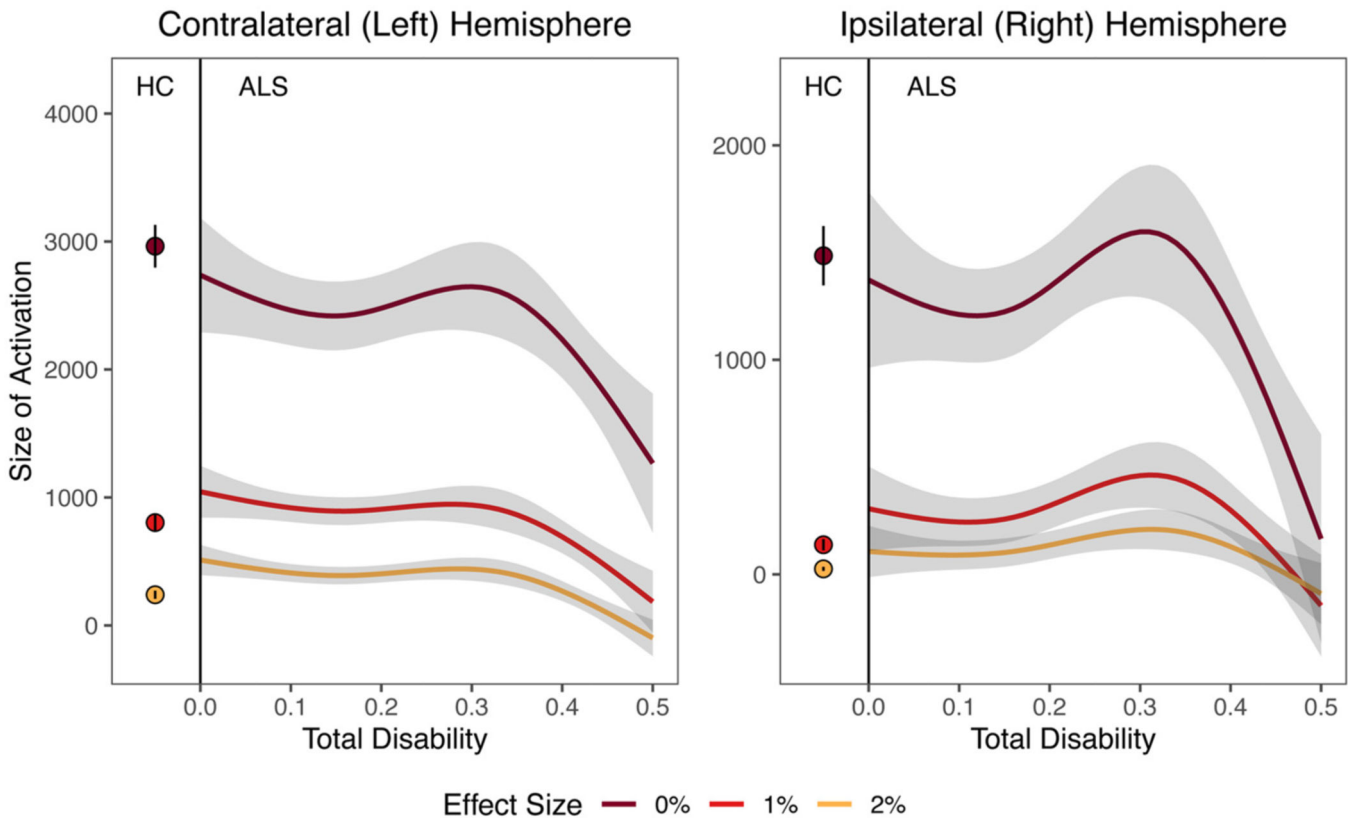

Fig. 3. Relationship of total ALS disability to the size of contralateral and ipsilateral activation in response to right hand clenching.

Values are based on the mixed effects model given in Eqn. (3) . The colored dots on the left-hand side of each plot represent the mean size of activation for HC participants, based on the random intercept model given in Eqn. (4), with error bars showing one standard error around the mean.

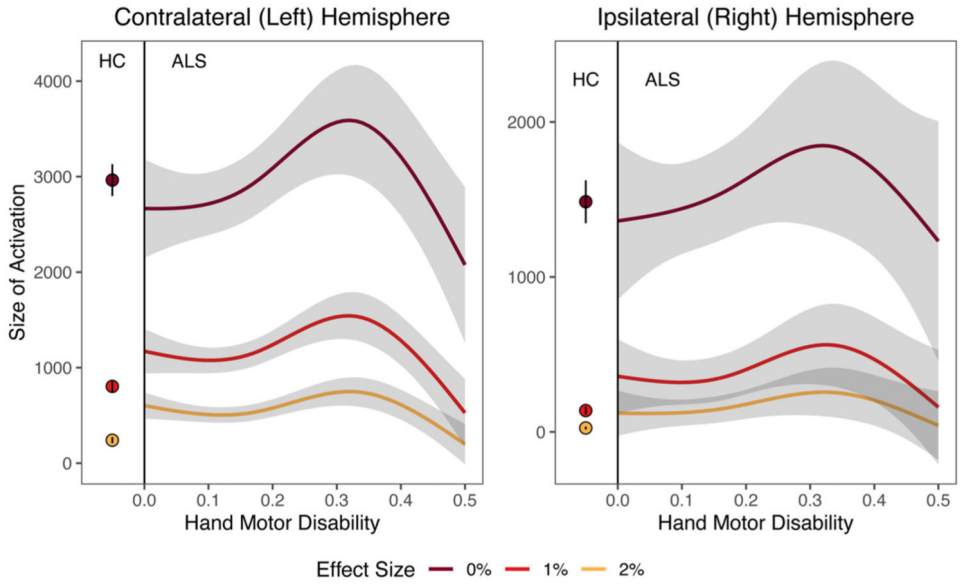

(a) Relationship between Hand Motor Disability and size of activation during right hand clenching.

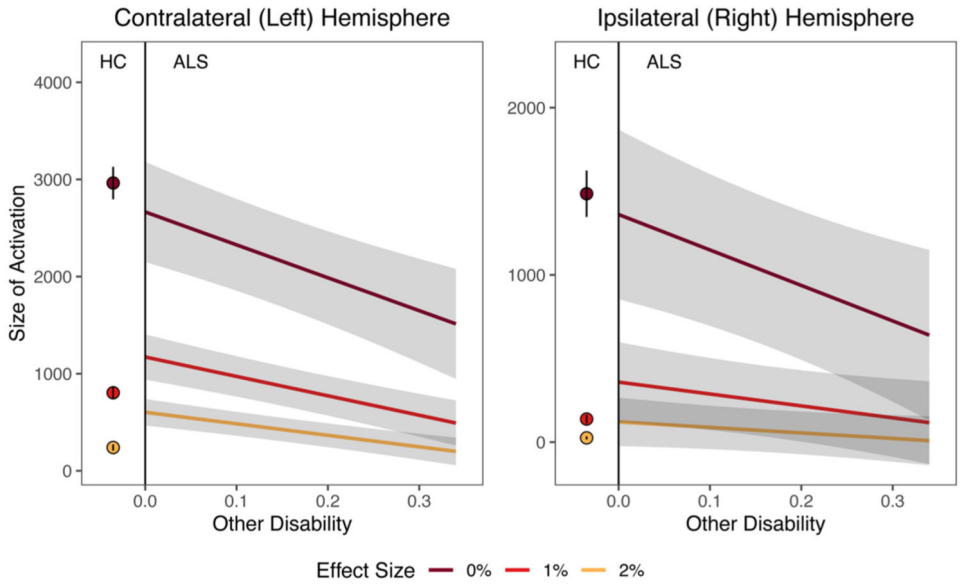

(b) Relationship between Other Disability and size of activation during right hand clenching.

Fig. 4. Relationship between the size of activation and hand motor disability and other disability in ALS.

Values are based on the mixed effects model given in Eqn. (3) . The predictor variables are *Hand Motor Disability* and *Other Disability*. The range of the x-axes represent up to the 90th quantile of each predictor. Shaded bands show one standard error around the mean. The colored dots on the left-hand side of each plot represent the mean size of activation for HC participants, based on the random intercept model given in Eqn. (4), with error bars showing one standard error around the mean. The curves shown in panel (a) reveal an

inverted-U-shaped relationship between size of activation and *Hand Motor Disability*; panel (b) shows decreasing size of activation associated with other aspects of disability.

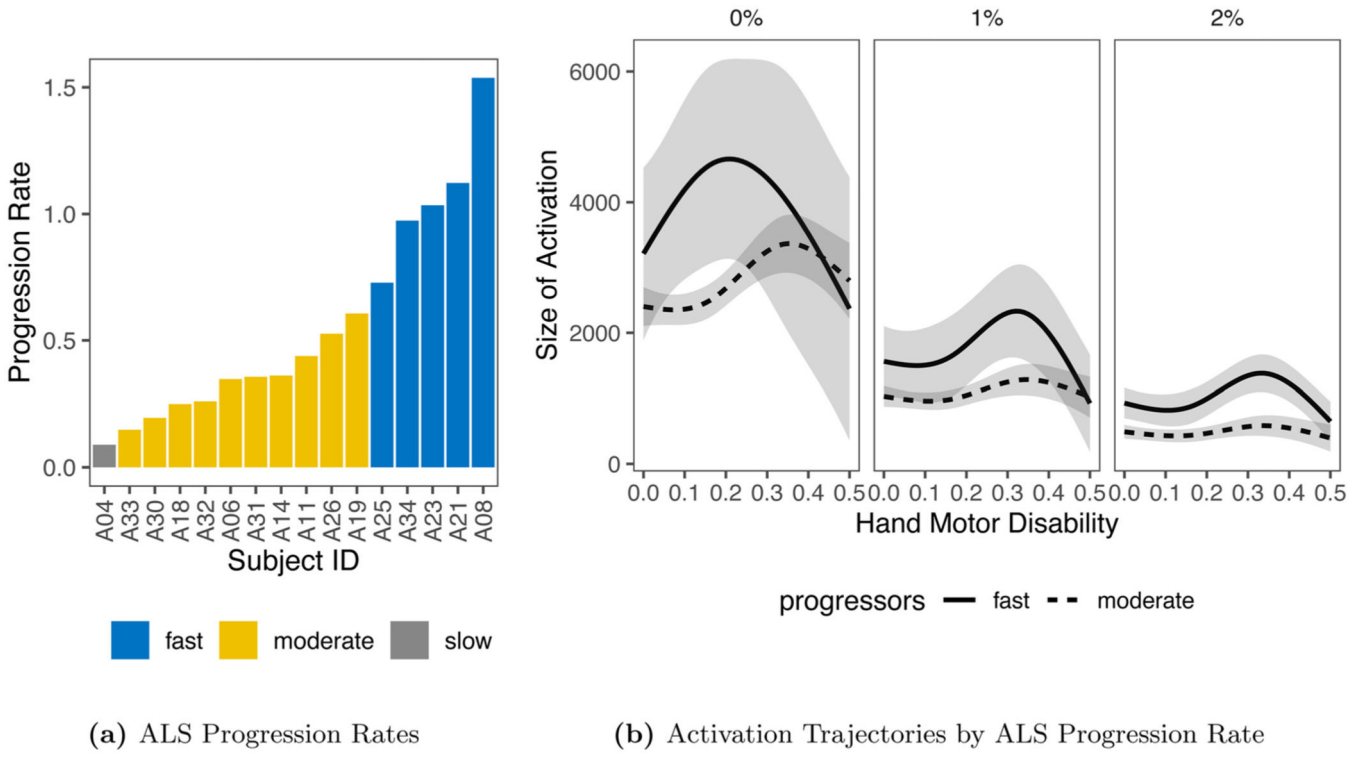

(a) ALS Progression Rates (b) Activation Trajectories by ALS Progression Rate

Fig. 5. Relationship between activation size and hand motor disability by ALS progression rate.

(a) Disability progression rate of ALS subjects and classification. **(b)** Coefficient curves for the size of contralateral activation in response to right hand clenching, based on the model in Eqn. 3 stratified by progression rate. Shaded bands show one standard error around the mean. Different panels correspond to the effect sizes 0%, 1% and 2% signal change. The overall shape is consistent with Fig. 4. However, fast progressors tend to peak higher and have higher baseline size of activation than moderate progressors. Furthermore, for the 0% effect size, the fast progressors tend to peak at an earlier stage of hand motor disability. Corresponding plots for ipsilateral activation are given in the Supplementary Materials and show similar patterns.

Table 1

ALS patient demographics.

ID	Sex	Onset Age	MSO	Onset Region	CBS	Dom. Hand
A04	M	58.4	4.0	LL	17	R
A06	M	51.9	18.8	LH	NA	R
A08	M	64.0	7.5	LH, RH	NA	R
A11	M	56.7	13.3	bulbar	9	R
A14	M	54.2	11.2	RH	18	R
A18	F	58.6	32.6	all limbs	9	R
A19	F	66.9	10.0	bulbar	14	R
A21	M	65.9	10.6	LL, RL	9	R
A23	M	55.6	12.8	bulbar	6	R
A25	M	53.6	12.1	bulbar	13	R
A26	M	56.3	23.5	bulbar, limb	17	R
A30	M	58.2 *	60.9 *	LL	12	R
A31	F	61.2	55.4	bulbar	12	R
A32	M	42.5	55.4	LH, RH	13	R
A33	F	54.0	15.7	LH	16	R
A34	M	54.8	14.4	LH	18	R

MSO = months between patient-reported onset of symptoms and the first scan.

* Patient A30 progressed from primary lateral sclerosis (PLS) to ALS; MSO based on clinical note indicating symptom onset date related to ALS. LH = left hand, RH = right hand, LL = left leg, RL = right leg. CBS = Cognitive Behavioral Screen. NA indicates CBS was not collected for that subject. Maximum possible score of 20, scores below 17 may suggest cognitive impairment, and scores below 10 suggest probable ALS with frontotemporal dementia (FTD). Scores are from date of first scan, except A04 (taken at 6th scan), A18, A 23, A26, A32, and A34 (2nd scan); Dom. Hand = dominant hand, as measured by the Edinburg Inventory.

Table 2

Progression Rate Groups.

Progression Rate	Progression Rate Range	ALS Participants
Slow	< 0.1 per month	A04
Moderate	0.1 to 0.69 per month	All other ALS participants
Fast	≥ 0.7 per month	A08, A21, A23, A25, A34

Progression rate was calculated as the average decrease in ALSFRS-R score (from the maximum value of 48, representing no disability) per month from disease onset to the last visit of each subject. The five fast progressors are those seen as exhibiting early decline in Fig. 1.